nature photonics

ARTICLES
https://doi.org/10.1038/s41566-018-0106-7

Real-time full-field characterization of transient dissipative soliton dynamics in a mode-locked laser

P. Ryczkowski[1,3], M. Närhi[1,3], C. Billet[2,3], J.-M. Merolla[2], G. Genty[1] and J. M. Dudley[2*]

Dissipative solitons are remarkably localized states of a physical system that arise from the dynamical balance between nonlinearity, dispersion and environmental energy exchange. They are the most universal form of soliton that can exist, and are seen in far-from-equilibrium systems in many fields, including chemistry, biology and physics. There has been particular interest in studying their properties in mode-locked lasers, but experiments have been limited by the inability to track the dynamical soliton evolution in real time. Here, we use simultaneous dispersive Fourier transform and time-lens measurements to completely characterize the spectral and temporal evolution of ultrashort dissipative solitons as their dynamics pass through a transient unstable regime with complex break-up and collisions before stabilization. Further insight is obtained from reconstruction of the soliton amplitude and phase and calculation of the corresponding complex-valued eigenvalue spectrum. These findings show how real-time measurements provide new insights into ultrafast transient dynamics in optics.

When operating in their steady-state regime, mode-locked lasers produce highly stable pulse trains, which have found widespread applications in photonics and many other areas of science[1–3]. However, mode-locked lasers can also exhibit complex instabilities when detuned from steady state or as stable mode-locking develops from noise[4–6]. These instabilities are of particular interest in passively mode-locked fibre lasers, as they reveal a rich landscape of dissipative soliton dynamics[7–10]. Dissipative solitons are the most universal class of localized soliton state in physics, existing for an extended period of time in the presence of nonlinearity and dispersion, even while parts of the structure can experience gain and loss[7]. Although there is an extensive theoretical literature on fibre laser dissipative solitons, experiments have been more limited, and often restricted to measurements using only fast photodetectors[6,9,11–13]. These experiments have certainly provided insight into the laser operation, but the limited available detector resolution has generally precluded detailed characterization of the underlying dynamics.

Recent years, however, have seen dramatic advances in the real-time measurement of non-repetitive optical signals[14–25]. The first method to see widespread use was the dispersive Fourier transform (DFT), which has yielded real-time spectral measurements of optical fibre rogue waves, modulation instability and supercontinuum generation[14–18]. More recently, the DFT has been applied to study the spectral properties of mode-locked lasers, revealing novel decoherence and soliton explosions in a fibre laser[19,20], and wavelength evolution dynamics in a Kerr-lens Ti:Sapphire laser[21]. In addition, soliton dynamics in the Kerr-lens Ti:Sapphire laser have also been studied using a modified DFT adapted for real-time spectral interferometry[22]. In parallel with these spectral measurements, the development of a temporal analogue of a spatial thin lens has resulted in real-time pulse intensity measurements with subpicosecond resolution[23]. This time-lens technique has been used in studies of incoherent soliton propagation in optical turbulence[24], and stochastic breather emergence in modulation instability[25].

Here, we report the first simultaneous use of real-time DFT and time-lens techniques to characterize the unstable evolution of dissipative solitons in a mode-locked fibre laser. One particular finding is the observation of transient coherent multi-soliton states, a previously experimentally unobserved feature of soliton fibre lasers associated with short-lived soliton molecules that grow from noise and rapidly decay. In addition, phase retrieval allows reconstruction of the full field (intensity and phase) of the measured pulses and calculation of the corresponding complex nonlinear eigenvalue spectrum. These results provide a unique picture of the internal evolution of dissipative solitons, and we anticipate the wide application of our approach in the optimization of lasers for improved stability. More generally, we believe that our results will stimulate wide use of simultaneous real-time temporal and spectral characterization as a standard measurement technique in ultrafast optics.

Results

Our experiments studied the transient turn-on dynamics of a saturable absorber mode-locked fibre laser configured (in stable operation) to generate pulses of ~4.5 ps duration at 1,545 nm with 20 MHz repetition rate (that is, a cavity round-trip time of 50 ns). The laser cavity has net anomalous dispersion and in steady-state operation, frequency-resolved optical gating measurements confirmed that the stable output pulses were well-fitted by a hyperbolic secant profile and were transform limited with a uniform temporal phase[26]. We used a commercial laser system in our experiments to highlight the practical utility of this technique in source development, and we selected the laser turn-on phase as a readily-accessible regime that displays rich dynamics.

We characterized the turn-on dynamics using both direct photodiode detection as well as simultaneous DFT and time-lens measurements (see Methods for full details). Figure 1 shows results using direct photodiode detection. Specifically, Fig. 1a plots the envelope of the pulses measured with reduced detection bandwidth to capture a time window of 130 ms, corresponding to 2.6 million

[1]Laboratory of Photonics, Tampere University of Technology, Tampere, Finland. [2]Institut FEMTO-ST, UMR 6174 CNRS-Université Bourgogne Franche-Comté, Besançon, France. [3]These authors contributed equally: P. Ryczkowski, M. Närhi and C. Billet. *e-mail: john.dudley@univ-fcomte.fr

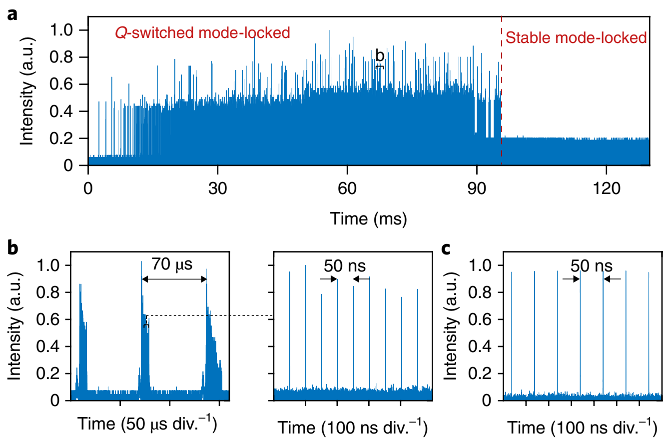

Fig. 1 | Direct photodetector measurement of transient laser dynamics. **a**, Results recorded with reduced bandwidth (20 MHz) detection illustrating the ~100 ms transient regime of *Q*-switched mode-locked operation before stable mode-locking. The region labelled 'b' in the time trace is shown in more detail in **b**. The total time record shown corresponds to 2.6 million round trips. **b**, Results from separate measurements using 30 GHz bandwidth detection, showing how the laser output during the *Q*-switched mode-locked regime consists of transient bursts of temporal width ~10 µs separated by ~70 µs period. The expanded view shows how unstable mode-locked pulses at 50 ns period are generated under each burst. **c**, Results using 30 GHz detection but in the stable mode-locked regime, showing a regular train of pulses with constant intensity. The time axis divisions (div.) are as indicated.

cavity round trips. The figure clearly reveals an ~100 ms transient regime of *Q*-switched mode-locked operation before the appearance of a stable pulse train. Figure 1b shows a separate measurement of a portion of the transient regime as indicated, but here using 30 GHz detection bandwidth so that it is possible to resolve a series of ~10 µs bursts separated by a ~70 µs period. The expanded view in Fig. 1b shows how under each burst, an irregular train of mode-locked pulses (at 50 ns period) is present. In contrast with this unstable regime, Fig. 1c shows measurements in the stable mode-locked regime using 30 GHz detection, to illustrate a regular pulse train of constant intensity. Of course, such complex transient dynamics have been seen in both numerical and experimental studies of a range of other passively mode-locked lasers[27–34], but we include these measurements here for completeness. The key point is that, even with a detection bandwidth of 30 GHz, the temporal width of the pulses seen in the photodiode intensity record is ~30 ps, precluding any detailed study of the underlying soliton dynamics in the transient regime. It is this limitation that we overcome with our simultaneous real-time DFT and time-lens measurements.

Figure 2 shows the setup used. Light from the fibre laser output was split into two paths and sent to the real-time DFT and time-lens acquisition arms. Real-time spectral measurements used a standard DFT setup[18] with spectral resolution of ~0.3 nm. The time-lens setup was similar to that described in ref. [25] and was capable of real-time measurements spanning a temporal window up to 60 ps duration and with an effective temporal resolution of 400 fs. Both DFT and time-lens signals were recorded using a high storage capacity digital oscilloscope, with data acquisition triggered by the time-lens signal detected after the laser was turned on. We could simultaneously measure spectral and temporal intensity profiles over a maximum of 400 cavity round trips (see Methods).

We recorded multiple data sequences to examine the spectral and temporal soliton dynamics both in the *Q*-switched mode-locked and the stable mode-locking regime. We begin in Fig. 3a–d by showing results for the stable mode-locking regime, where as expected the spectral (Fig. 3a) and temporal (Fig. 3b) intensity profiles are constant with round trip. The extracted spectral and temporal widths and the integrated pulse energy are shown on the right; the small (noise) variations in these figures is of the order of the experimental resolution of the spectral and temporal measurements.

Although the ability to measure both temporal and spectral intensity in real time is itself a highly significant advance, we extend this technique further using Gerchberg–Saxton phase retrieval[35,36] to recover the corresponding complex electric field of each pulse (see Methods). These results are shown in Fig. 3c, where we plot the retrieved intensity (left axis) and phase (right axis) revealing the soliton characteristics of near-uniform phase. Access to the full complex electric field allows us to calculate the associated wavelength–time spectrogram (see Methods), and these results are shown in Fig. 3d, confirming the localized soliton-like nature of the pulses. Figure 3e–h shows similar results, but taken from a data sequence just before the regime of stable mode-locking. Here, over a relatively small number of round trips, we see significant modulation in both the measured spectral and temporal amplitudes, as well as energy variation of ~30%. This 'breathing' of the intracavity pulses just before the onset of stability is a known property of dissipative soliton dynamics in mode-locked lasers[21], but our results here characterize it completely in both the time and frequency domains.

Dissipative solitons are known to display a wide range of dynamics[7–9], and to capture this behaviour we repeated experiments by restarting the laser many times and varying the trigger hold-off time to scan different points of the transient regime (see Methods). The general dynamics were similar for all bursts, showing the emergence of multiple pulses from noise followed by subsequent decay, but the detailed pulse evolution varied significantly between measurements. A selection of typical results is shown in Fig. 4 (note that evolution with round trip is plotted from top to bottom). The figure shows spectral (Fig. 4a,e,i) and temporal (Fig. 4b,f,j) intensity profiles (with energy shown on the right), as well as retrieved intensity and phase (Fig. 4c,g,k) and spectrograms (Fig. 4d,h,l) . Also note that energy is not constant in this turn-on regime[12]. We first discuss Fig. 4a–d, which shows an initial noisy field splitting into three distinct pulses (of duration ~5 ps) that propagate together over ~100 round trips. Each pulse displays a well-localized temporal intensity peak, and the pulses are mutually coherent as shown by the distinct modulation in the corresponding spectrum. Significantly, the pulse separation does not vary over ~100 round trips as the pulses evolve without seeming to interact before decaying. Figure 4e–h shows a qualitatively different case. Here, two pulses emerge, but rather than propagating without interacting, they undergo attraction and eventually collide, displaying a more complex nonlinear phase profile at this point. Figure 4i–l in contrast shows another example of burst evolution where a combination of the above dynamics are observed with the emergence of three solitons.

From analysis of multiple *Q*-switched bursts, we have been able to identify that the emergence of multi-pulse states consisting of two or three distinct soliton-like structures is a typical feature of this transient regime. Such bound coherent soliton states in a laser are referred to as soliton molecules[37], but in contrast to previous studies of stable or periodic behaviour[22,38], our results (in both time and frequency domains) reveal a regime of short-lived growth and decay that has not previously been directly observed. We also note that the interaction dynamics within the soliton molecule can be very complex, depending on the pulse frequencies, their temporal separation, as well as their initial amplitudes and phases[37,39–42]. In this context, the spectrogram plots in Fig. 4 are useful in interpreting the observed behaviour. In Fig. 4a–d for example, the central frequencies of the constituent pulses change very little with propagation, whereas in

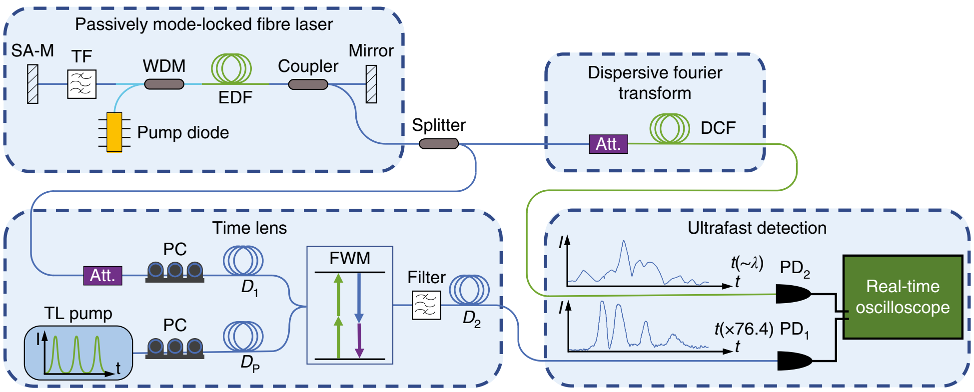

Fig. 2 | Experimental setup. Pulses from a passively mode-locked fibre laser are directed to DFT and time-lens stages. The laser cavity includes a saturable absorber mirror (SA-M) and a tunable filter (TF). The DFT used 850 m of dispersion compensating fibre (DCF) and a 35 GHz photodiode (PD_2). The time lens uses two dispersive steps (D_1 and D_2) and a silicon waveguide that applies a quadratic temporal phase through four-wave mixing (FWM) with pulses (chirped in fibre D_p) from a 100 MHz femtosecond fibre laser (TL pump). The time-lens signal is extracted from the FWM spectrum by an optical filter and measured using a 13 GHz photodiode (PD_1). Both PD_1 and PD_2 were input to a 30 GHz real-time oscilloscope channel. Attenuation (Att.) was used to avoid nonlinear effects, and polarization control (PC) ensured optimal signal from the time-lens. See Methods for values of D_1, D_2 and D_p and other details. WDM, wavelength-division multiplexer; EDF, erbium-doped fibre; TL, time lens. The illustrative plot axes show intensity (I), time (t) and wavelength (λ).

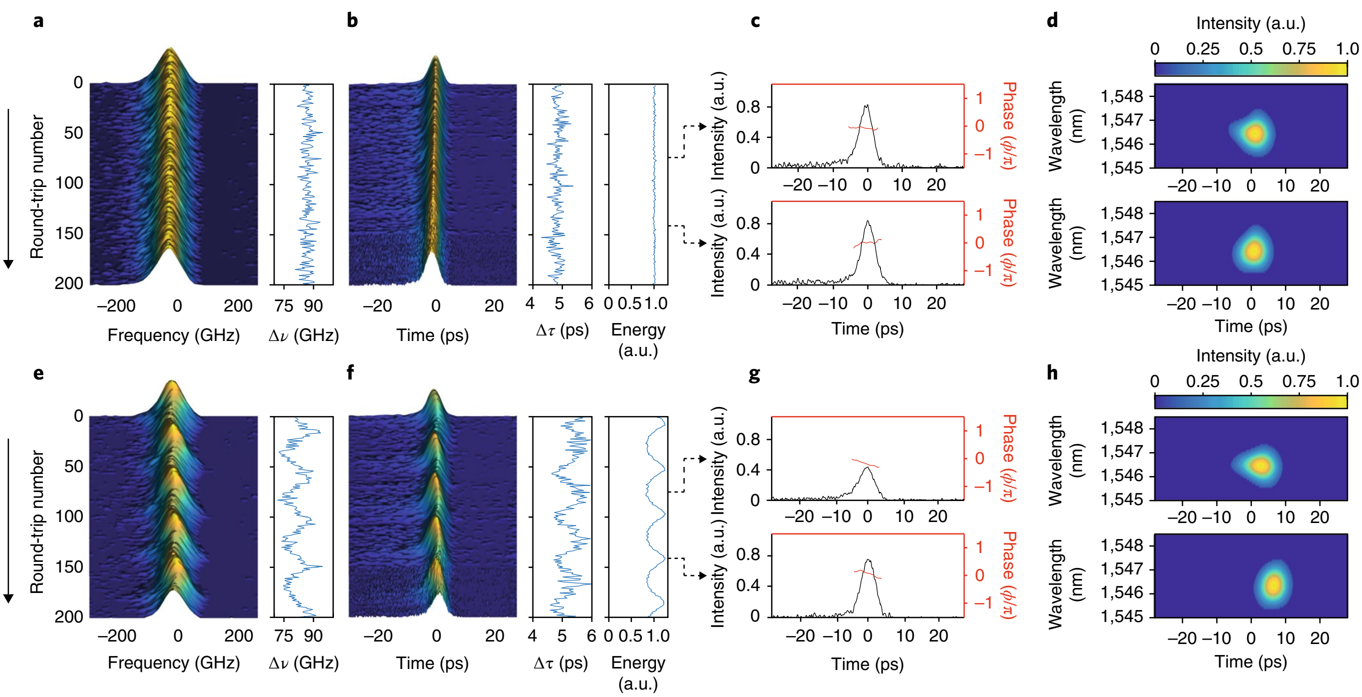

Fig. 3 | Real-time spectral and temporal characterization near stability. a–h, Experimental measurements over 200 round trips for stable (**a**–**d**) and breathing (**e**–**h**) mode-locking regimes. For each regime, we show: measured spectral intensity, with the extracted spectral width $\Delta\nu$ shown on the right (**a**,**e**); measured temporal intensity, with the extracted temporal width $\Delta\tau$ and energy shown on the right (**b**,**f**); corresponding temporal intensity (black, left axis) and phase (red, right axis) extracted using the Gerchberg–Saxton algorithm for pulses at the round-trip evolution points indicated by arrows (**c**,**g**); for each of the extracted pulses in **c** and **g**, the calculated wavelength–time spectrogram (**d**,**h**). The colour scale shows spectrogram intensity in linear arbitrary units normalized relative to the maximum.

Fig. 4e–l the two pulses that eventually merge display initial frequency differences of 0.4 and 0.5 nm, respectively, but their frequencies evolve with propagation until they eventually coincide at the point of pulse collision.

The ability to reconstruct the complex electric field from the measured intensity and phase allows calculation of derived quantities that yield additional physical insights. In particular, it is possible to apply numerical techniques from scattering theory to yield spectral eigenvalue portraits of the pulse structures[43–47]. More specifically, according to inverse scattering theory, any initial condition of the nonlinear Schrödinger equation (NLSE) evolves into a combination of solitons plus non-solitonic (quasi-nonlinear) oscillating wave packets, and it is the parameters of the solitons formed that are derived via the inverse scattering transform[47]. Although inverse

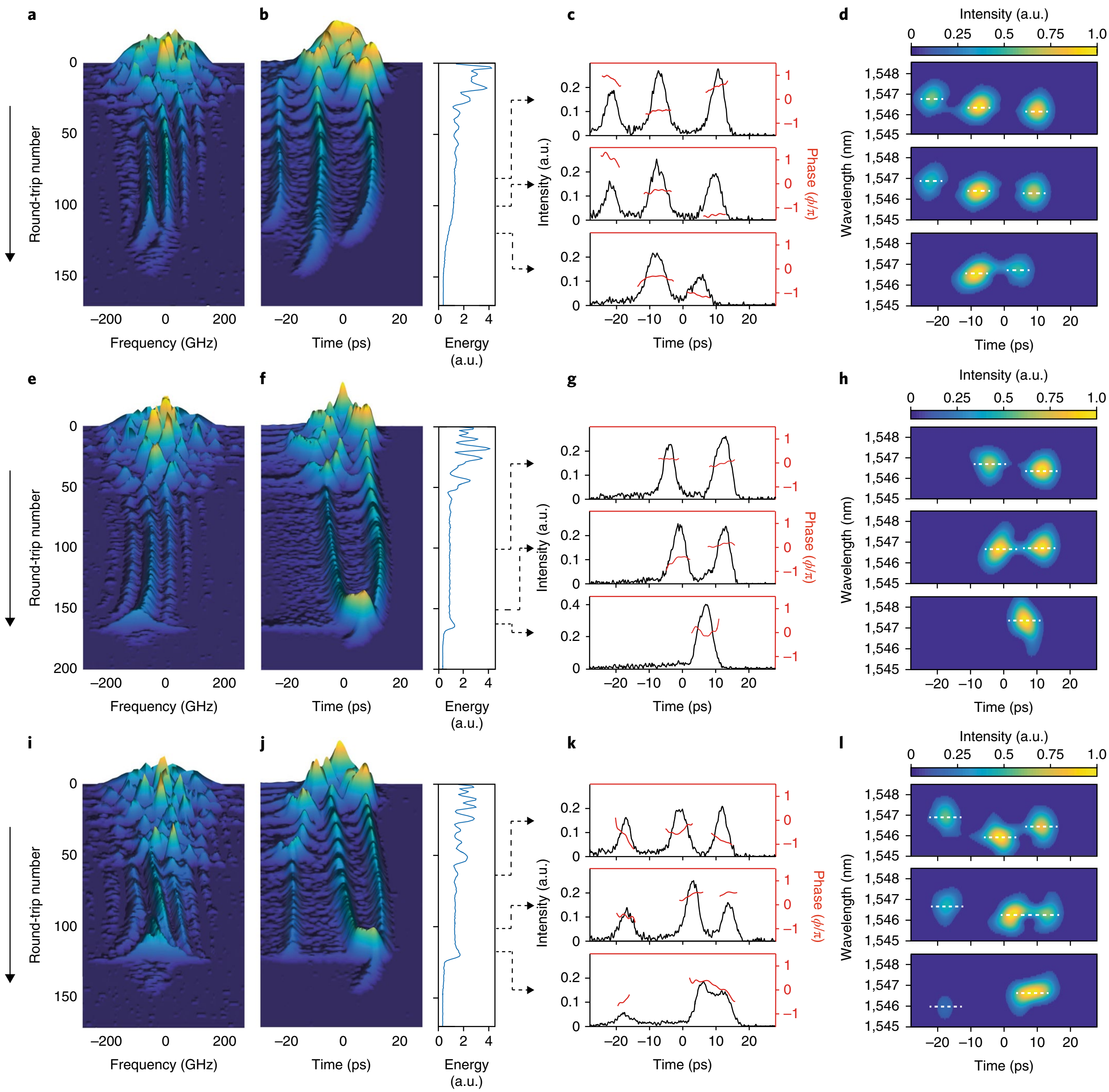

Fig. 4 | Real-time spectral and temporal characterization of complex dynamics. a–l, Results showing real-time spectral and temporal characterization for a non-interacting triplet of three solitons over 170 round trips (**a–d**), more complex collision dynamics of a soliton double pulse over 200 round trips (**e–h**) and a combination of a single soliton and a two-pulse collision over 170 round trips (**i–l**). For each case, we show: measured spectral intensity (**a**,**e**,**i**); measured temporal intensity with integrated energy shown on the right (**b**,**f**,**j**); corresponding temporal intensity (black, left axis) and phase (red, right axis) extracted using the Gerchberg–Saxton algorithm for pulses at the round-trip evolution points indicated by arrows (**c**,**g**,**k**); for the extracted pulses in **c**, **g** and **k**, the calculated wavelength–time spectrogram (**d**,**h**,**l**). The dashed line in the spectrograms indicate the pulse central frequencies and the colour scale shows spectrogram intensity in linear arbitrary units normalized relative to the maximum.

scattering in fibre optics has generally been used to obtain analytic solutions to the NLSE, there has been recent interest in using associated numerical techniques (often called the nonlinear Fourier transform) to study rogue-wave dynamics[48] and to overcome channel limits in optical communications[49].

With this approach applied to the intensity and phase measurements of pulses from the mode-locked fibre laser, the calculated eigenspectra for several cases are shown in Fig. 5. Here the red dots show the discrete eigenspectrum for the normalized pulse intensity profiles shown as insets. Here ψ is the normalized pulse envelope that generates the scattering potential, τ is the time variable and ζ is the calculated eigenvalue (see Methods). In this case, we associate the stable pulse regime in Fig. 3a–d with solitons having eigenvalues at $\zeta = \pm 0.5i$ in the complex plane, physically equivalent to injecting them in an optical fibre with initial conditions corresponding to a fundamental soliton. Based on the measurements in Fig. 3a–d, we normalize the intensities of other measured pulses with respect to these ideal solitons and perform direct scattering analysis to

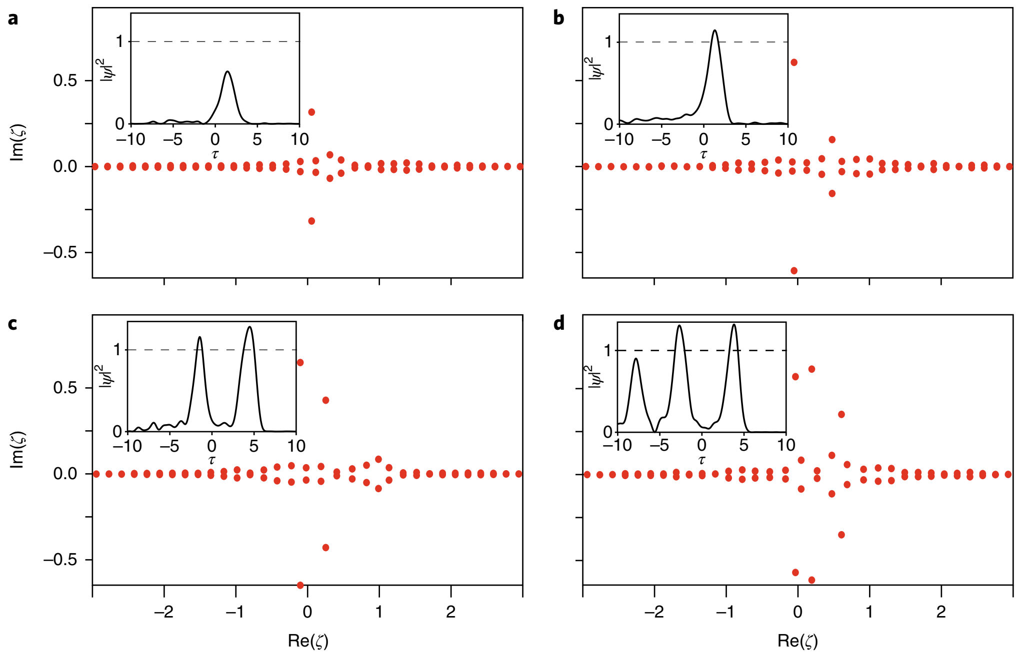

Fig. 5 | Eigenvalue content of unstable solitons. a–d, The red dots show the calculated eigenspectrum corresponding to the normalized intensity profiles shown as insets (ψ is amplitude, τ is time). Results in **a** and **b** correspond to the two points in the breather cycle shown in Fig. 3e–h. As the pulse intensity varies below and above the unity value of a fundamental soliton, the eigenvalue Im(ζ) varies below and above ±0.5. Results in **c** correspond to the double soliton in Fig. 4e–h where we see two eigenvalues with Im(ζ) ~±0.5. Results in **d** correspond to the three-soliton case in Fig. 4a–d where we see three eigenvalues with Im(ζ) around ±0.5. Note that the intensity profiles correspond to results shown in Figs. 3 and 4 but are smoothed for clarity when shown as insets. The dashed line in the insets shows the maximum intensity of an ideal soliton.

determine the corresponding more complex eigenvalue spectrum (see Methods and Supplementary Information).

We first consider the results in Fig. 5a,b, which correspond to single pulses at two points of the breather cycle shown in Fig. 3g. In each case the scattering analysis yields one distinct eigenvalue, and we see that as the pulse intensity varies below and above the unity value of a normalized fundamental soliton (dashed black line), the eigenvalue Im(ζ) also varies below and above the ideal soliton value of ±0.5. In other words, the variation in the eigenvalue reflects the breathing of the pulse properties in this regime. We also note the residual 'eye-like' structure in the eigenvalue spectrum corresponding to the small pedestal in the intensity distribution (see Supplementary Information).

Figure 5c,d considers evolution that is more complex. Figure 5c plots the eigenvalue spectrum for the double-soliton pulse shown in Fig. 4g, where the direct scattering procedure yields two discrete eigenvalues, both with Im(ζ) ~±0.5. Figure 5d shows results for the three-soliton case in Fig. 4a–d and here we see two discrete eigenvalues with Im(ζ) ~±0.5 and a third eigenvalue at a slightly lower value. As in the breathing regime of Fig. 3e–h, we note the presence of a residual pedestal around the zero of the real axis in the nonlinear spectrum. In all cases, the clear separation of the eigenvalues from the real axis indicates that this regime before steady-state mode-locking creates discrete pulse complexes, similar to those seen with multiple bound solitons[7–9]. This is an important insight that the nonlinear Fourier transform reveals directly.

Discussion

Dissipative nonlinear systems can be highly complex, but it is clear that recent years have seen tremendous advances in understanding their behaviour through theory and numerical modelling. Of course, it is essential that theoretical and numerical results are carefully compared with experiment, and to this end, the study reported here makes a significant contribution. The results obtained explicitly show the complex temporal and spectral dynamics that can occur during transient burst behaviour, and in particular, reveal the transient emergence and decay of coherent multi-soliton states. We anticipate that these findings will stimulate theoretical work to understand the underlying governing physical mechanisms, building on the extensive existing literature[37] and including possible long-range interactions from transverse acoustic waves generated through soliton-induced electrostriction[50].

More generally, our results also highlight the use of simultaneous time-lens and DFT measurements for complete intensity and phase characterization. When compared with other full-field measurement techniques such as frequency-resolved optical gating[36] or spectral phase interferometry for direct electric-field reconstruction[51], simultaneous time-lens and DFT measurements operate at orders of magnitude lower peak power (typically ~1 W peak power is required by the time lens, <100 mW peak power by the DFT). Moreover, acquisition is possible at the 20 MHz repetition rate of the laser, and can be extended to gigahertz repetition rates with asynchronous operation of the time lens. To our knowledge, no other technique can be used to provide real-time characterization and intensity and phase information of ultrafast instabilities of a nature and at power levels such as those reported here, although we note that real-time measurements of turbulence in optical fibre propagation have recently been reported using tens of microjoule pump pulses to create a temporal hologram[52]. The temporal resolution in our setup is ultimately limited by the phase-matching properties of the silicon waveguide and the duration of the pump pulse in the time-lens system, but resolutions in the ~200 fs range have been reported[53] and further improvement might be expected with dedicated waveguide dispersion-engineering.

A further area of significance concerns our use of the nonlinear Fourier transform to calculate the eigenspectrum of the pulses generated from the mode-locked fibre laser. The calculated spectra clearly show the presence of local soliton content, which provides a new window into the physics of the underlying laser dynamics. We also believe our results will motivate interest in broader applications of the nonlinear Fourier transform for characterizing ultrashort pulses[54,55]. In optics, we anticipate particular interest in real-time spectral and temporal studies of nonlinear single-pass propagation dynamics in optical fibres such as rogue waves and modulation instability.

Methods

Methods, including statements of data availability and any associated accession codes and references, are available at https://doi.org/10.1038/s41566-018-0106-7.

Received: 24 July 2017; Accepted: 18 January 2018;
Published online: 05 March 2018

References

1. French, P. M. W. The generation of ultrashort laser pulses. *Rep. Prog. Phys.* **58**, 169–267 (1995).
2. Keller, U. Recent developments in compact ultrafast lasers. *Nature* **424**, 831–838 (2003).
3. Hänsch, T. W. Nobel Lecture: Passion for precision. *Rev. Mod. Phys.* **78**, 1297–1309 (2006).
4. Abraham, D., Nagar, R., Mikhelashvili, V. & Eisenstein, G. Transient dynamics in a self-starting passively mode-locked fiber-based soliton laser. *Appl. Phys. Lett.* **63**, 2857–2859 (1993).
5. Dudley, J. M., Loh, C. M. & Harvey, J. D. Stable and unstable operation of a mode-locked argon laser. *Quantum Semiclass. Opt.* **8**, 1029–1039 (1996).
6. Hönninger, C., Paschotta, R., Morier-Genoud, F., Moser, M. & Keller, U. *Q*-switching stability limits of continuous wave passive mode locking. *J. Opt. Soc. Am. B* **16**, 46–56 (1999).
7. Akhmediev, N. & Ankiewicz, A. (eds) *Dissipative Solitons*, *Lecture Notes in Physics*, Vol. 661 (Springer-Verlag, Berlin, Germany, 2005).
8. Grelu, P. & Akhmediev, N. Dissipative solitons for mode-locked lasers. *Nat. Photon.* **6**, 84–92 (2012).
9. Grelu, P. (ed.) *Nonlinear Optical Cavity Dynamics: From Microresonators to Fiber Lasers* (Wiley, Berlin, Germany, 2016).
10. Turitsyn, S. K. et al. Dissipative solitons in fiber lasers. *Phys. Usp.* **59**, 642–668 (2016).
11. Flynn, M. B., O'Faolain, L. & Krauss, T. F. An experimental and numerical study of *Q*-switched mode-locking in monolithic semiconductor diode lasers. *IEEE J. Quant. Electron.* **40**, 1008–1013 (2004).
12. Schlatter, A., Zeller, S. C., Grange, R., Paschotta, R. & Keller, U. Pulse-energy dynamics of passively mode-locked solid-state lasers above the *Q*-switching threshold. *J. Opt. Soc. Am. B* **21**, 1469–1478 (2004).
13. Lecaplain, C., Grelu, P., Soto-Crespo, J. M. & Akhmediev, N. Dissipative rogue waves generated by chaotic pulse bunching in a mode-locked laser. *Phys. Rev. Lett.* **108**, 233901 (2012).
14. Goda, K. & Jalali, B. Dispersive Fourier transformation for fast continuous single-shot measurements. *Nat. Photon.* **7**, 102–112 (2013).
15. Solli, D. R., Ropers, C., Koonath, P. & Jalali, B. Optical rogue waves. *Nature* **450**, 1054–1057 (2007).
16. Godin, T. et al. Real time noise and wavelength correlations in octave-spanning supercontinuum generation. *Opt. Express* **21**, 18452–18460 (2013).
17. Solli, D. R., Herink, G., Jalali, B. & Ropers, C. Fluctuations and correlations in modulation instability. *Nat. Photon.* **6**, 463–468 (2012).
18. Wetzel, B. et al. Real-time full bandwidth measurement of spectral noise in supercontinuum generation. *Sci. Rep.* **2**, 882 (2012).
19. Runge, A. F. J., Aguergaray, C., Broderick, N. G. R. & Erkintalo, M. Coherence and shot-to-shot spectral fluctuations in noise-like ultrafast fiber lasers. *Opt. Lett.* **38**, 4327–4330 (2013).
20. Runge, A. F. J., Broderick, N. G. R. & Erkintalo, M. Observation of soliton explosions in a passively mode-locked fiber laser. *Optica* **2**, 36–39 (2015).
21. Herink, G., Jalali, B., Ropers, C. & Solli, D. R. Resolving the build-up of femtosecond mode-locking with single-shot spectroscopy at 90 MHz frame rate. *Nat. Photon.* **10**, 321–326 (2016).
22. Herink, G., Kurtz, F., Jalali, B., Solli, D. R. & Ropers, C. Real-time spectral interferometry probes the internal dynamics of femtosecond soliton molecules. *Science* **356**, 50–54 (2017).
23. Kolner, B. H. & Nazarathy, M. Temporal imaging with a time lens. *Opt. Lett.* **14**, 630–632 (1989).
24. Suret, P. et al. Single-shot observation of optical rogue waves in integrable turbulence using time microscopy. *Nat. Commun.* **7**, 13136 (2016).
25. Närhi, M. et al. Real-time measurements of spontaneous breathers and rogue wave events in optical fibre modulation instability. *Nat. Commun.* **7**, 13675 (2016).
26. Billet, C., Dudley, J. M., Joly, N. & Knight, J. C. Intermediate asymptotic evolution and photonic bandgap fiber compression of optical similaritons around 1550 nm. *Opt. Express* **13**, 3236–3241 (2005).
27. Soto-Crespo, J. M., Akhmediev, N. & Town, G. Continuous-wave versus pulse regime in a passively mode-locked laser with a fast saturable absorber. *J. Opt. Soc. Am. B* **19**, 234–242 (2002).
28. Schreiber, T., Ortaç, B., Limpert, J. & Tünnermann, A. On the study of pulse evolution in ultra-short pulse mode-locked fiber lasers by numerical simulations. *Opt. Express* **15**, 8252–8262 (2007).
29. Sarukura, N. & Ishida, Y. Pulse evolution dynamics of a femtosecond passively mode-locked Ti:sapphire laser. *Opt. Lett.* **17**, 61–63 (1992).
30. Vodonos, B. et al. Experimental study of the stochastic nature of the pulsation self-starting process in passive mode locking. *Opt. Lett.* **30**, 2787–2789 (2005).
31. Li, H., Ouzounov, D. G. & Wise, F. W. Starting dynamics of dissipative-soliton fiber laser. *Opt. Lett.* **35**, 2403–2405 (2010).
32. Zinkiewicz, Ł., Ozimek, F. & Wasylczyk, P. Witnessing the pulse birth-transient dynamics in a passively mode-locked femtosecond laser. *Laser Phys. Lett.* **10**, 125003 (2013).
33. Ghiu Lee, C., Kim, J., Kim, S. & Petropoulos, P. Transient response of a passively mode-locked Er-doped fiber ring laser. *Opt. Commun.* **356**, 161–165 (2015).
34. Wang, Z. et al. *Q*-switched-like soliton bunches and noise-like pulses generation in a partially mode-locked fiber laser. *Opt. Express* **24**, 14709–14716 (2016).
35. Gerchberg, R. W. & Saxton, W. O. A practical algorithm for the determination of the phase from image and diffraction plane pictures. *Optik* **35**, 237–246 (1972).
36. Trebino, R. *Frequency-Resolved Optical Gating: The Measurement of Ultrashort Laser Pulses* (Wiley, Berlin, Germany, 2000).
37. Grelu, P. & Soto-Crespo, J. M. in *Dissipative Solitons: From Optics to Biology and Medicine, Lecture Notes in Physics*, Vol. 751 (eds Akhmediev, N. & Ankiewicz, A.) 137–173 (Springer, Berlin, Heidelberg, 2008).
38. Krupa, K., Nithyanandan, K., Andral, U., Tchofo-Dinda, P. & Grelu, P. Real-time observation of internal motion within ultrafast dissipative optical soliton molecules. *Phys. Rev. Lett.* **118**, 243901 (2017).
39. Tang, D. Y., Zhao, B., Zhao, L. M. & Tam, H. Y. Soliton interaction in a fiber ring laser. *Phys. Rev. E* **72**, 16616 (2005).
40. Roy, V., Olivier, M. & Piché, M. Pulse interactions in the stretched-pulse fiber laser. *Opt. Express* **13**, 9217–9223 (2005).
41. Akhmediev, N., Soto-Crespo, J. M., Grapinet, M. & Grelu, P. Dissipative soliton interactions inside a fiber laser cavity. *Opt. Fib. Tech.* **11**, 209–228 (2005).
42. Akhmediev, N., Soto-Crespo, J. M. & Town, G. Pulsating solitons, chaotic solitons, period doubling, and pulse coexistence in mode-locked lasers: complex Ginzburg-Landau equation approach. *Phys. Rev. E* **63**, 56602 (2001).
43. Zakharov, V. E. & Shabat, A. B. Exact theory of two-dimensional self-focusing and one-dimensional self-modulation of waves in nonlinear media. *Sov. Phys. JETP* **34**, 62–69 (1972).
44. Akhmediev, N. & Ankiewicz, A. *Solitons: Non-linear Pulses and Beams* (Chapman and Hall, London, UK, 1997).
45. Osborne, A. R. *Nonlinear Ocean Waves and the Inverse Scattering Transform* (Elsevier, London, UK, 2010).
46. Agrawal, G. P. *Nonlinear Fiber Optics* (Elsevier, Oxford, UK, 2013).
47. Turitsyn, S. K. & Derevyanko, S. A. Soliton-based discriminator of noncoherent optical pulses. *Phys. Rev. A* **78**, 063819 (2008).
48. Randoux, S., Suret, P. & El, G. Inverse scattering transform analysis of rogue waves using local periodization procedure. *Sci. Rep.* **6**, 29238 (2016).
49. Turitsyn, S. K. et al. Nonlinear Fourier transform for optical data processing and transmission: advances and perspectives. *Optica* **4**, 307–322 (2017).
50. Jang, J. K., Erkintalo, M., Murdoch, S. G. & Coen, S. Ultraweak long-range interactions of solitons observed over astronomical distances. *Nat. Photon.* **7**, 657–663 (2013).
51. Iaconis, C. & Walmsley, I. A. Spectral phase interferometry for direct electric-field reconstruction of ultrashort optical pulses. *Opt. Lett.* **23**, 792–794 (1998).
52. Tikan, A., Bielawski, S., Szwaj, C., Randoux, S. & Suret, P. Phase and amplitude single-shot measurement by using heterodyne time-lens and ultrafast digital time-holography. *Nat. Photon.* https://doi.org/10.1038/s41566-018-0113-8 (2018).
53. Salem, R., Foster, M. A. & Gaeta, A. L. Application of space–time duality to ultrahigh-speed optical signal processing. *Adv. Opt. Photon.* **5**, 274–317 (2013).

54. Sugavanam, S., Kamalian, M., Peng, J., Prilepsky, J. E. & Turitsyn, S. K. Experimentally characterized nonlinear fourier transform of a mode-locked fibre laser. In *Conference on Lasers and Electro-Optics Europe and the European Quantum Electronics Conference* EF-2.6 (Optical Society of America, 2017).
55. Narhi, M., Ryczkowski, P., Billet, C., Genty, G. & Dudley, J. M. Ultrafast simultaneous real time spectral and temporal measurements of fibre laser modelocking dynamics. In *Conference on Lasers and Electro-Optics Europe and the European Quantum Electronics Conference* EE-3.5 (Optical Society of America, 2017).

Acknowledgements

This work was supported by the Agence Nationale de la Recherche project LABEX ACTION ANR11-LABX-0001-01, the Region of Franche-Comté Project CORPS and the Academy of Finland (Grants 267576 and 298463). The authors also thank K. V. Reddy for providing technical details concerning the soliton operating regime of the Pritel laser used in these experiments.

Author contributions

All authors participated in all the experimental work and data analysis reported, and in the writing and review of the final manuscript. G.G. and J.M.D. planned the research project and provided overall supervision.

Competing interests

The authors declare no competing interests.

Additional information

Supplementary information is available for this paper at https://doi.org/10.1038/s41566-018-0106-7.

Reprints and permissions information is available at www.nature.com/reprints.

Correspondence and requests for materials should be addressed to J.M.D.

Publisher's note: Springer Nature remains neutral with regard to jurisdictional claims in published maps and institutional affiliations.

Methods

Experimental setup. The fibre laser used in our experiments was a commercial Pritel FFL-500 model using a linear Fabry-Perot cavity configuration shown in Fig. 2, similar to that described in ref. [56], but with a 978 nm pump laser and Er:doped fibre gain medium. Mode-locking is sustained by a 2-μm-thick bulk saturable absorber (InGaAs on InP substrate) contact bonded to one of the cavity mirrors. The steady-state mode-locking dynamics are dominated by soliton propagation effects because of the net anomalous dispersion in the cavity, with the generation of hyperbolic secant-like pulses of flat phase in stable operation.

We implemented the DFT technique using 850 m of dispersion compensating fibre with group velocity dispersion of 100 ps nm^{-1} km^{-1} and dispersion slope 0.33 ps nm^{-2} km^{-1} at 1,550 nm. We attenuated the input to the dispersion compensating fibre to ensure linear propagation, and confirmed the fidelity of the time-stretching technique by comparing the DFT spectrum with that measured using an optical spectrum analyser (Anritsu MS9710B) in the stable mode-locked regime. The real-time DFT signal was measured by a 35 GHz photodiode (New Focus 1474 A) connected to a 30 GHz channel of a real-time oscilloscope (LeCroy 845 Zi-A, 80 GS s^{-1}), resulting in a spectral resolution of 0.3 nm.

The time-lens measurements used a commercial Picoluz UTM-1500 system described previously[24] with a temporal magnification factor of 76.4. The values of the dispersion for the input and output propagation segments were $D_1 = 4.16$ ps nm^{-1} and $D_2 = 318$ ps nm^{-1}, respectively. The associated magnification is given by $|M| = D_2/D_1$. The analogue to spatial propagation across a thin lens is obtained from the temporal quadratic phase developed on the pulse under test through four-wave mixing from a linearly chirped pump pulse (100 MHz Menlo C-Fiber Sync and P100-EDFA). The linear chirp here on the pump arises from propagation in a fibre segment of dispersion D_p. To satisfy the thin-lens imaging condition ($2/D_p = 1/D_1 + 1/D_2$), the system parameters are chosen such that the pump dispersion D_p is around twice the dispersion experienced by the signal D_1 during its input propagation segment. The signal at the time-lens output is input to 13 GHz photodiode (Miteq 135GE) and measured with the 30 GHz channel of the real-time oscilloscope at a sampling rate of 80 Gs s^{-1}, resulting in an effective 400 fs temporal resolution over a (demagnified) time window of 60 ps. The temporal window is determined by the pump pulse duration used in the time lens to impose the required quadratic chirp via four-wave mixing in a highly nonlinear Si waveguide[52]. In stable mode-locked operation it is possible to synchronize the 20 MHz laser under study with the 100 MHz pump laser, but this is not the case when studying transient dynamics because of significant noise that prevents the detection of a well-defined 20 MHz harmonic for repetition-rate locking. The time lens is therefore operated in asynchronous mode with free-running acquisition triggered by the arrival of the time-lens signal, although this limits the number of round trips that can be simultaneously measured to ~400 (as there is a walk-off between the *Q*-switched mode-locked pulses relative to the time-lens gate).

To obtain representative datasets at different times of the transient regime evolution, we performed multiple measurements with different delays between the turn-on time of the fibre laser and the time-lens trigger, restarting the laser between each measurement. We can use this approach to characterize different phases of the pulse evolution in the transient regime because: (1) the measurement window of 400 round trips (20 μs) is longer than that of the typical transient bursts that have lifetimes of only 200–300 round trips (10–15 μs), and (2) we can use a variable hold-off trigger for different measurements and thus capture different phases of the overall transition phase that lasts over many millions of round trips (~100 ms). Although the limited measurement window precludes the real-time characterization of the full 100 ms transient regime with subpicosecond resolution, this technique allows recording of many key dynamical features. We also emphasize that we performed many hundreds of measurements under conditions of different laser restarts to study different phases of the laser dynamics and consistently obtained results similar to those in Fig. 3e–h (breathing) and Fig. 4 (multiple pulse behaviour).

In more detail, the triggering scheme was as follows. We employed a two-stage triggering scheme to the ultrafast oscilloscope with an adjustable hold-off time between the two trigger signals. The first trigger was obtained from the first measured DFT pulse (that is, the first *Q*-switched mode-locked burst in the full transient evolution cycle), which starts the hold-off countdown time. Once the hold-off time has passed, the actual acquisition of the temporal profile is triggered from the first signal at the time-lens output. By performing repeated measurements for different laser restarts with hold-off times varying in the range 1–100 ms, we could readily examine the dynamical properties of bursts throughout the full transition regime.

Finally, we note that because the optical path lengths of the DFT and time-lens steps were different, the delay between time-lens and DFT records was calibrated (in a separate measurement) by comparing the arrival times on the oscilloscope of a characteristic intensity pattern imprinted onto a continuous-wave (CW) laser. This allowed us to match without ambiguity the real-time temporal and spectral intensity profiles of the dissipative solitons during their transient evolution.

Phase retrieval. To retrieve the phase based on the simultaneously measured temporal and spectral intensity profiles, we used an approach based on the Gerchberg–Saxton algorithm[35]. The algorithm constructs an initial guess for the profile of the electric field $E_g(t)$ using the temporal intensity measured in experiments $I_M(t)$, on which an initial random temporal phase $\phi_{\text{rand}}(t)$ is applied to give: $E_g(t) = \sqrt{I_M(t)}\, e^{i\phi_{\text{rand}}(t)}$. This temporal field is then transformed to the spectral domain, yielding the corresponding spectral amplitude $S(\omega)$ and spectral phase $\varphi(\omega)$ through FT $[E_g(t)] = \sqrt{S(\omega)}\, e^{i\varphi(\omega)}$, where FT here indicates the Fourier transform. The next step involves keeping the calculated spectral phase but replacing the calculated spectral amplitude with the measured spectral amplitude ($\sqrt{S_M}$), that is, $\sqrt{S_M(\omega)}\, e^{i\varphi(\omega)}$. This updated spectral profile is transformed back into the time domain (using an inverse Fourier transform) where the same approach is used: we keep the calculated temporal phase but replace the calculated amplitude with that from experiment $\sqrt{I_M(t)}$. This procedure is iteratively repeated until the root mean square error between the retrieved intensity profiles and measurements is lower than a chosen value. We found that a target error of 3×10^{-5} yielded good results. The performance of the algorithm (that is, its speed of convergence) could be improved using a thresholding approach whereby the experimental temporal and spectral constraints are applied only where the measured intensities were at values greater than −20 dB from the maximum. For values outside this range, an amplitude multiplicative factor of 10^{-3} was applied. Algorithm stagnation was detected if there was no change in the retrieval error (before the target value) over several iterations, and in such cases, adding a small additional random phase was found to lead to renewed convergence. The phase-retrieval capabilities of the algorithm was extensively tested using numerically generated pulses with complex properties similar to those seen in experiments. In addition, the reproducibility of the algorithm was examined by running it multiple times on the same experimental data, and checking that all retrieval runs led to the same results. Examples of retrievals using numerical data and additional information can be found in the Supplementary Information.

Spectrogram calculation. Access to the full field in amplitude and phase allows us to calculate a frequency (or wavelength)–time spectrogram. For a pulse with complex field $E(t)$, the spectrogram can be interpreted as the modulus squared of a short-time Fourier transform, a function that represents the intensity and phase content of the pulse in the time and frequency domains simultaneously. The spectrogram is defined by:

$$S(\omega,\tau) = \left| \int_{-\infty}^{\infty} E(t)g(t-\tau)e^{-i\omega t}\mathrm{d}t \right|^2 \quad (1)$$

with $g(t-\tau)$ a variable delay gate function with delay value τ. Here t and ω are time and angular frequency, respectively. The spectrogram thus shows the spectra of a series of time-gated portions of $E(t)$ and provides a highly intuitive and visual means of interpreting the frequency–time content of a complex field. In our calculation of the spectrograms from experimental data, we used a Gaussian pulse gate function of duration (full width at half maximum) of 4 ps.

Nonlinear Fourier transform. The nonlinear Fourier transform (also known as the direct scattering transform) is a mathematical procedure that identifies and quantifies soliton content in a given pulse structure. In fact, any initial condition of the NLSE evolves into a combination of solitons plus quasi-linear oscillating wave packets, and the scattering transform can be used to determine the number of solitons formed and their associated parameters. In particular, we consider a system described by the NLSE in normalized form:

$$i\frac{\partial\psi}{\partial\xi} + \frac{1}{2}\frac{\partial\psi}{\partial\tau^2} + |\psi|^2\psi \quad (2)$$

where ψ is the normalized pulse envelope that generates the scattering potential, ξ is the propagation variable and τ is the time variable in a co-moving frame. The associated scattering problem yields the following system:[42]

$$\begin{aligned}\frac{\partial v_1}{d\tau} + \psi v_2 &= \zeta v_1 \\ \frac{\partial v_2}{d\tau} + \psi^* v_1 &= \zeta v_2\end{aligned} \quad (3)$$

where v_1 and v_2 are the amplitudes of the waves scattered by the potential induced by ψ, and ζ is the corresponding complex eigenvalue. For our results, we consider the laser output pulses in Fig. 3a–d as associated with solitons having eigenvalues at $\zeta = \pm 0.5i$ in the complex plane. This would be physically equivalent to injecting them in an optical fibre with the initial conditions of a fundamental soliton, obtained for example by appropriate adjustment of the injected power. This case corresponds to amplitude $|\psi| = 1$, and the field profiles corresponding to the other pulses analysed were normalized relative to this value. Standard numerical techniques (matrix methods) were used to determine the eigenvalue spectrum[57].

Data availability. The data that support the plots within this paper and other findings of this study are available from the corresponding author upon reasonable request.

References

56. Reddy, K. V. et al. A turnkey 1.5 μm picosecond Er/Yb fiber laser. In *Conference on Optical Fiber Communication (OFC), OSA Technical Digest Series* PD17 (Optical Society of America, 1993).
57. Wahls, S. & Poor, H. V. Fast numerical nonlinear Fourier transforms. *IEEE Trans. Inf. Theory* **6**, 6957–6974 (2015).